Springer

KSME

Journal of Mechanical Science and Technology 24 (8) (2010) 1697~1707
www.springerlink.com/content/1738-494x
DOI 10.1007/s12206-010-0518-x

Evaluation of friction coefficient using simplified deformation model of plastic hemispherical contact with a rigid flat †

Daw-Kwei Leu*

Technology and Science Institute of Northern Taiwan, Department of Mechanical Engineering, No. 2, Xueyuan Road, Beitou, Taipei, Taiwan 112, R.O.C.

(Manuscript Received March 6, 2010; Revised April 6, 2010; Accepted April 20, 2010)

Abstract

This work evaluates the friction coefficient using the model of plastic hemispherical contact against a rigid flat. The fractional profile of an ellipsoid is utilized to describe the deformed hemispherical shape, and simultaneously define the contact area ratio. Particularly, an adhesion factor is defined to assess the junction ability of asperity adhesion under compressive loading. Additionally, the complex process of contact is assumed as a series of contact states changing from fracture to shearing. The friction coefficient, which obeys the constant friction law, is then derived as a function of interference and strain hardening exponent via adhesion theory. Finally, a comparison of friction coefficient is made with the published experiment, showing that the calculated value is larger than the experimental value. Some practical conclusions are presented and a conceptual understanding of contact friction is provided.

Keywords: Adhesion; Contact; Deformation; Friction

1. Introduction

The most significant effect on surface contact is resistance when sliding, which is the meaning of contact friction. Contact friction is due to forces that arise from the interactions of asperities in sliding contact. Blau [1] identified the characteristics of friction coefficients, such as the measurement and usage of static and kinetic friction coefficients, and sources of frictional resistances. Since all surfaces of mechanical parts are to some degree rough once manufactured, the modeling of contact between these rough surfaces becomes extremely important and leads to an enhanced understanding of contact friction between surfaces. When two rough surfaces are pressed together under a load, only the asperities on the surface are in contact. Thus, the asperities of surfaces often have very high loads, often causing surface yielding. Therefore, purely elastic contact models of rough surfaces are not always adequate under severe loading.

Notably, two different models are typically utilized to analyze contacting asperities. One model is indentation loading in which a rigid sphere penetrates a deformed plane, and the other model is the reverse case, in which a deformed sphere is loaded against a rigid flat; these models are employed to investigate the characteristics of contact. This work is concerned with hemispherical contact against a rigid flat.

Greenwood and Williamson [2] pioneered the study of frictionless contact between a hemisphere and a rigid flat (the GW model) applied the Hertz contact solution to model an entire contact surface of elastic asperities. To supplement the GW model, many elastic-plastic asperity models have been devised. Many plastic contact models are based on the Abbott and Firestone model [3], but neglect volume conservation of plastic deformation. Plastic contact of surfaces is a fundamental problem in the contact mechanics of severe loading.

Any understanding of friction must be rooted in an understanding of contact mechanics. During contact, asperity interactions combined with adhesion always occur and are often the primary cause of friction. Chang et al. [4] applied the GW model to an elastic-plastic contact (CEB) model to estimate the static friction of two rough surfaces in contact. Elastic-plastic finite element solutions, such as the sliding inception of a spherical contact developed by Kogut and Etsion [5] and the elastic-plastic contacting rough surfaces developed by Kogut and Etsion [6], are applied to predict a better static friction coefficient than that predicted by Chang et al. [4]. Etsion et al. [7] recently conducted an experiment to investigate the elastic-plastic contact area and static friction of a deformable sphere on a rigid flat. Brizmer et al. [8] theoretically analyzed the behavior of an elastic–plastic contact between a deformable sphere and a rigid flat under combined normal and tangential loading with full stick contact condi-

† This paper was recommended for publication in revised form by Associate Editor Dae-Eun Kim

* Corresponding author. Tel.: +886 2 28927154
E-mail address: dkleu@tsint.edu.tw

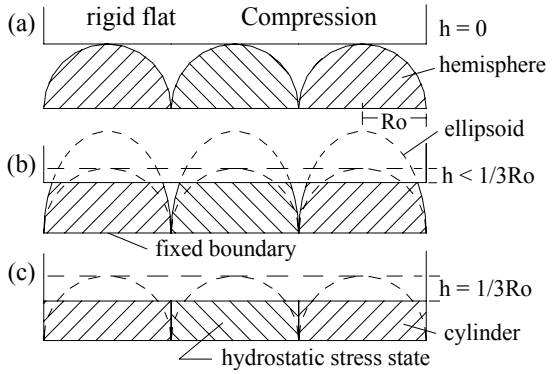

Fig. 1. Contact model for hemispherical contact against a rigid flat, showing three compressive loading processes: (a) hemisphere, $h = 0 \rightarrow$ (b) ellipsoid, $h < R_0/3 \rightarrow$ (c) cylinder, $h = R_0/3$, in which a single hemispherical contact is used to represent the whole contact condition for all hemispheres (asperities) are identical in contact on the surface.

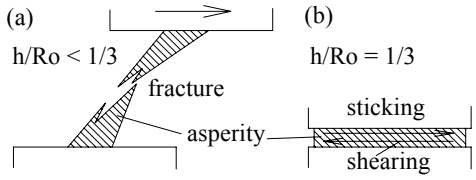

Fig. 2. The schemes of (a) fracture and (b) sticking states in friction contact.

tion. Ovcharenko et al. [9] experimentally studied the elastic-plastic contact between a deformable sphere and a rigid flat during pre-sliding. Cohen et al. [10] studied the elastic-plastic spherical contact of rough surfaces under combined normal and tangential loading with full stick contact condition.

A proper friction coefficient is very difficult to obtain. Therefore, conceptual understanding of the friction process is now essential to an accurate estimation of the friction coefficient. The contribution of this work is the mathematical representation of friction under dry friction for practical and analytical applications. The most popular and simplest constant friction coefficient of the Amonton-Coulomb friction model is applied in this study. An extended model, including material properties and surface contact characteristics, is proposed on a model of a hemispherical contact against a rigid flat. A fractional profile of an ellipsoid is utilized to describe the deformed shape of a hemisphere; the real contact area ratio is defined simultaneously. The normal contact pressure is assumed as a mean stress. Additionally, an adhesion factor is defined to measure the junction ability of asperity contact. It is assumed that the friction process is a series of contact states changing from fracture to pure shearing. The effects of several factors are examined using the proposed contact model.

2. Basic analysis

Fig. 1 describes schematically the contact processes of rough surfaces during compression. In the contact layer, the hardened and polished surface, such as the tool surface, is replaced by a rigid flat, and the raw and rough surface, such as the deformable material surface, is replaced with a deformable hemisphere. Additionally, it is assumed that the surface asperities are homogeneously distributed on the contact surface and do not interfere with adjacent asperities. Thus, a single asperity contact model can be generally approached in this manner. In the processes of compression (Figs. 1(a)-(c)), the shape of the deformed hemisphere is approximated by a fractional ellipsoid distribution to facilitate an analytical solution, which is a key feature of this work. Additionally, the deformed hemisphere becomes a cylinder (Fig. 1(c)) in the final stage of compression based on the constant volume law of plasticity. Of course, the surface contamination and the formation of oxide films are neglected in this model. For deformation behavior, the elastic deformation is neglected in deformation analysis.

The conventional adhesion theory, the first modern explanation of friction, was developed by Bowden and Tabor [11], which posits that contact adhesion during surface interaction causes friction resistance in which the combined effect of normal pressure and shear stress is considered at the contact area of an asperity junction. In this work, the constant friction coefficient, such as Amonton-Coulomb friction law extensively used in analysis and application, is defined as

$$\mu = \frac{F_t}{N} \tag{1}$$

where the tangential force, F_t, broke the friction junction and normal force, N, induced contact. On the real contact area, A_r, the constant friction coefficient can be written as

$$\mu = \frac{F_t}{N} = \frac{\tau_f}{p_r}\frac{A_r}{A_r} = \frac{\tau_f}{p_r} = \frac{\alpha\tau_s}{p_r} \tag{2}$$

The friction stress $\tau_f = \alpha\tau_s$ is based on the work of Shaw [12] that τ_s is maximum shear stress and p_r is contact pressure. In identifying the constructs of the contact layer, it is believed that the junction fracture of an adhesive asperity results in resistance to sliding (Fig. 2 (a)). In this situation, τ_s can be replaced by

$$\tau_s \rightarrow C_a\sigma_f \tag{3}$$

where the fracture stress, σ_f, is defined as the true tensile strength (in terms of true stress) $\sigma_u = Kn^n$ based on the condition that necking deformation (plastic instability) begins at maximum load of simple tension test, and C_a is defined as an adhesion factor with a range of $1 \sim 1/\sqrt{3}$, in which $C_a = 1$ is the sliding case ($\tau_s \rightarrow \sigma_u$) and $C_a = 1/\sqrt{3}$ is the sticking case (Fig. 2(b)) in which $\tau_s = \sigma_u/\sqrt{3}$ on von Mises yield criteria. The constant friction coefficient, μ, can then be described as

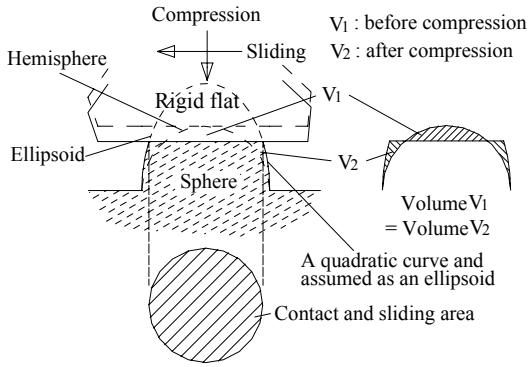

Fig. 3. Deformed shape of hemisphere contacting with a rigid flat.

$$\mu = \frac{\alpha \tau_s}{p_r} = \alpha \cdot C_a \cdot \frac{1}{\left(\frac{p_r}{\sigma_u}\right)} \tag{4}$$

Clearly, the constant friction coefficient, μ, can be defined as a function of dimensionless parameters α, C_a and (p_r / σ_u), which are analyzed as follows.

2.1 The profile of a deformed hemisphere against a rigid flat

The shape of a deformed hemisphere is approximated as a fractional ellipsoid distribution, which is a feature of this work, and becomes a cylinder in the final stage (Fig. 1(a) to (c)). On this assumption, the equation of the ellipse for a 2-D section of an ellipsoid can be used,

$$\frac{x^2}{a^2} + \frac{y^2}{b^2} = 1 \tag{5}$$

where a $(= R_0)$ is the length of the fixed short axis of the ellipsoid (*i.e.* the radius of the hemisphere) and b is the length of the long axis of the ellipsoid that varies with compressive loading.

The constant volume law of plastic deformation is obeyed by $V_1 = V_2$, such that the squeezed volume at a certain interference h (V_1) equals the spread volume around the periphery of the contact plane (V_2) (Fig. 3), in which

$$V_1 = \frac{1}{3}\pi h^2 (3R_0 - h) \tag{6}$$

$$V_2 = \left\{\frac{2}{3}\pi R_0^2 b - \frac{\pi}{3} R_0^2 \frac{(b - R_0 + h)^2}{b^2}\left[3b - (b - R_0 + h)\right]\right\} - \left[\frac{2}{3}\pi R_0^3 - \frac{1}{3}\pi h^2 (3R_0 - h)\right] \tag{7}$$

Then, b under the condition of $V_1 = V_2$ is

$$b^2 = \frac{(R_0 - h)^3}{R_0 - 3h} \tag{8}$$

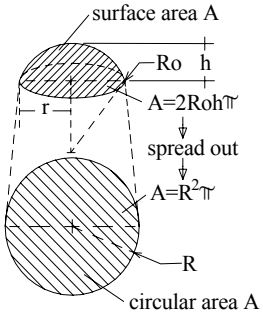

Fig. 4. The surface area of a spherical cap is spread out in a plane as a circular area by a compressive loading of rigid flat.

The ellipse equation is then used to describe the profile of a deformed hemisphere at a certain interference h can be written as

$$\frac{x^2}{R_0^2} + \frac{y^2}{\left[\frac{(R_0 - h)^3}{R_0 - 3h}\right]} = 1 \tag{9}$$

$$\text{or } \frac{y}{R_0} = \sqrt{\left[1 - \left(\frac{x}{R_0}\right)^2\right] \frac{\left[1 - \left(\frac{h}{R_0}\right)\right]^3}{1 - 3\left(\frac{h}{R_0}\right)}} \tag{10}$$

Clearly, the ellipse equation is a function of interference h. The profile of the deformed hemisphere changed from an ellipsoid $(h < R_0/3)$ to a cylinder at the final stage $(h = R_0/3)$ within the range of $0 \le h \le R_0/3$. It is concluded that

(1) $h = 0$, $\frac{x^2}{R_0^2} + \frac{y^2}{R_0^2} = 1$, is a hemisphere before compression (Fig. 1 (a));

(2) $h < \frac{1}{3}R_0$, $\frac{x^2}{R_0^2} + \frac{y^2}{\left[\frac{(R_0 - h)^3}{R_0 - 3h}\right]} = 1$, has a fractional shape of an ellipsoid between $y = 0$ and $y = R_0 - h$ at a certain interference h (Fig. 1 (b)); and

(3) $h = \frac{1}{3}R_0$, $\frac{x^2}{R_0^2} = 1$, $\frac{x}{R_0} = \pm 1$, $y = \frac{2}{3}R_0$, is a cylinder in the final stage (Fig. 1(c)).

During the final stage, the deformed hemisphere changed into a cylinder, implying that the stress state will change into a hydrostatic stress state of compression. Under this condition, the final cylinder shape (radius, R_0; height, $2R_0/3$) at $h = R_0/3$ will not be compressed further because of the constraints resulting from the adjacent hemispheres.

2.2 The contact area ratio

In the proposed model, the contact area ratio is defined as

$$\alpha = \frac{A_r}{A_a} = \frac{\pi R'^2}{\pi R_0^2} \tag{11}$$

where A_r is the real contact area at a certain interference h corresponding to R' and A_a is the apparent area which equals the normal projective area of the hemisphere.

Substituting $x = R'$ and $y = R_0 - h$ into the ellipse equation, Eq. 9, yields

$$\frac{R'^2}{R_0^2} + \frac{(R_0 - h)^2}{\frac{(R_0 - h)^3}{R_0 - 3h}} = 1 \tag{12}$$

The contact area ratio at a certain interference h can then be obtained as $R_0 - 3h$

$$\alpha = \frac{R'^2}{R_0^2} = 1 - \frac{R_0 - 3h}{R_0 - h} = \frac{2h}{R_0 - h} = \frac{2\left(\frac{h}{R_0}\right)}{1 - \left(\frac{h}{R_0}\right)} \tag{13}$$

with interference ratio h / R_0.

At the interference range of $0 \le h \le R_0/3$, the contact area ratio is

(1) $\alpha = 0$ at $h = 0$ and $A_r = 0$;

(2) $\alpha < 1$ at $h < \frac{1}{3}R_0$ and $A_r < A_a$; and

(3) $\alpha = 1$ at $h = \frac{1}{3}R_0$ and $A_r = A_a$, as full contact.

The full contact state is defined as a sticking state, which corresponds to the hydrostatic stress state of compression in which only slipping via shearing can be induced.

2.3 Mean contact pressure and compressive load

At a certain level of interference h, we assume compressive stress induced by the contact area is a mean contact pressure. Additionally, the compressed hemisphere is simplified as an axial symmetrical stress element for axial symmetrical configuration. Under the constant volume law and axial symmetrical conditions of $\varepsilon_z + \varepsilon_\theta + \varepsilon_r = 0$ and $\varepsilon_\theta = \varepsilon_r$,

$$\varepsilon_z = -2\varepsilon_\theta = -2\ln\frac{R}{r} \tag{14}$$

where ε_r, ε_θ and ε_z are true strains in r, θ and z directions, respectively, and r and R are the radius of the compressed element before and after compression, respectively, at a certain level of interference h.

The effective strain, ε_e, and stress, σ_e, based on von Mises yield criteria of plastic deformation, can be written as

$$\varepsilon_e = 2\varepsilon_\theta = 2\ln\frac{R}{r} \tag{15}$$

and

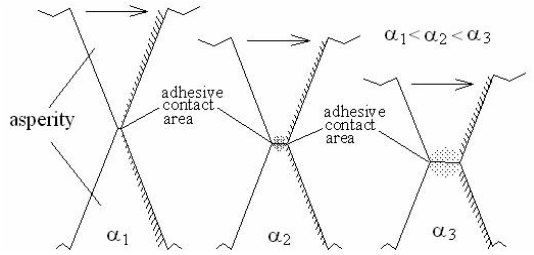

Fig. 5. The schemes of junction phenomenon for asperities contact; $C_a(\alpha_1) > C_a(\alpha_2) > C_a(\alpha_3)$.

$$\sigma_e = K\varepsilon_e^n = K\left(2\ln\frac{R}{r}\right)^n \tag{16}$$

From Fig. 4, radius r can be obtained

$$r = \sqrt{(2R_0 - h)h} \tag{17}$$

To obtain R, the surface area of a spherical cap with radius R_0 and height h (*i.e.* interference) prior to compression equals the corresponding circular area after compression is assumed and shown in Fig. 4. First, the surface area of spherical cap before compression at a certain h is

$$A = 2\pi R_0 h \tag{18}$$

Second, the circular area, the surface area of spherical cap spread in a plane, is

$$A = \pi R^2 \tag{19}$$

Radius R after compression can then be obtained by $A = 2\pi R_0 h = \pi R^2$,

$$R = \sqrt{2R_0 h} \tag{20}$$

The effective strain can be obtained by substituting R and r into Eq. (15),

$$\varepsilon_e = 2\varepsilon_\theta = 2\ln\frac{\sqrt{2R_0 h}}{\sqrt{(2R_0 - h)h}} = \ln\frac{2}{\left(2 - \frac{h}{R_0}\right)} \tag{21}$$

Thus, the mean contact pressure, p_r, on the contact area can be approximated as

$$p_r \approx \sigma_e = K\left(\ln\frac{2}{\left(2 - \frac{h}{R_0}\right)}\right)^n \tag{22}$$

or normalized as

$$\frac{p_r}{\sigma_u} = \frac{\left(\ln\frac{2}{\left(2 - \frac{h}{R_0}\right)}\right)^n}{n^n} \tag{23}$$

Thus, the compressive load at a certain interference ratio h/R_0 can be written as

$$F_p = A_r p_r = \pi R'^2 K \left[\ln \frac{2}{\left(2 - \frac{h}{R_0}\right)} \right]^n \tag{24}$$

$$= \pi R_0^2 K \left[\ln \frac{2}{\left(2 - \frac{h}{R_0}\right)} \right]^n \frac{2\frac{h}{R_0}}{1 - \frac{h}{R_0}}$$

or normalized as

$$\frac{F_p}{\pi R_0^2 K} = \frac{2\left(\frac{h}{R_0}\right)}{1 - \left(\frac{h}{R_0}\right)} \left[\ln \frac{2}{\left(2 - \frac{h}{R_0}\right)} \right]^n = F_m \tag{25}$$

which is a function of strain hardening exponent *n* and interference ratio h/R_0, where F_m is normalized compressive load.

2.4 Adhesion factor C_a

As is well known, micro fracture and shear slipping are always induced on the sliding contact surface of materials. Therefore, the junction ability of contact asperities needs a more detailed clarification that the junction ability decreases as contact area increases in the early contact stage because full junction is easily attained for contact between two whole sharp peaks of asperity which results in a complete deformation energy concentration, a very large energy density. On the other hand, in this early contact stage, the contact layer has a significant amount of space, and fracture stress primarily results from the broken junction, not shearing. Fig. 5 shows this phenomenon. This is something like the press operation of shearing of sheet metal forming with a large clearance between punch and die. Therefore, at the start of contact, fracture stress can be defined as $C_a\sigma_u$, in which $C_a = 1$ for a case of complete fracture resulting from full junction.

Therefore, while contact or compression increases, the contact area increases markedly, and deformation energy will be spread out on the increasing contact area and then transfer to the contact body. Thus, the energy per unit contact volume (or energy density) decreases and results in a poor contact junction. However, the asperities become reciprocally squeezed within the reduced space in the contact layer. Finally, full contact is achieved and the stress condition becomes a pure shearing state called a sticking state, which is something like the fine blanking process of sheet metal forming. In the final stage, fracture stress can be defined as $C_a\sigma_u$, in which $C_a = 1/\sqrt{3}$, fracture stress turns to maximum shear stress based on von Mises yield criteria, for a pure shearing case in a full contact sticking state.

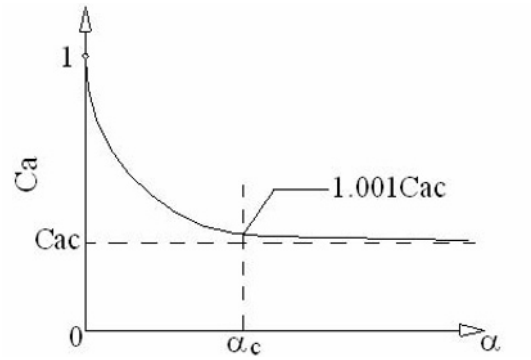

Fig. 6. The proposed distribution of adhesion factor C_a; $C_a = 1$ as $\alpha = 0$ and $C_a \approx C_{ac}$ as $\alpha = \alpha_c$.

Therefore, the adhesion factor can be defined as a function of α, another feature of this work,

$$C_a = C_{ac} + (1 - C_{ac}) e^{-c\alpha} \tag{26}$$

where $C_a = 1$ as $\alpha = 0$ and $C_a \to C_{ac}$ as $\alpha \to \infty$ (Fig. 6), and *c* is a constant.

To obtain the value of *c*, an acceptable error is assumed as 0.001 for full contact at $\alpha = \alpha_c = 1$. The constant *c* can then be acquired from the condition of $C_a = 1.001 C_{ac}$ at $\alpha = \alpha_c = 1$,

$$c = \ln\left[10^3 \left(\frac{1}{C_{ac}} - 1 \right) \right] \tag{27}$$

Obviously, the C_{ac} can be defined as $C_{ac} = 1/\sqrt{3}$. Then Eq. (26) can be written as,

$$C_a = \frac{1}{\sqrt{3}} + \left(1 - \frac{1}{\sqrt{3}}\right) e^{-\ln\left[10^3\left(\sqrt{3}-1\right)\right]\alpha} \tag{28}$$

and $1/\sqrt{3} \le C_a \le 1$.

Eq. (28) implies that

(1) $\alpha = 0$, $C_a = 1$, $\sigma_f \to \sigma_u$, full junction as a fracture case; and

(2) $\alpha = 1$, $C_a \approx C_{ac} = 1/\sqrt{3}$, $\sigma_f \to 1/\sqrt{3}\sigma_u = \tau_s$, full contact (or sticking state) as a shearing case.

2.5 The friction coefficient

From Eq. (4), the friction coefficient can be generalized as

$$\mu = \alpha \cdot C_a \cdot \left(\frac{p_r}{\sigma_u} \right)^{-1}$$

where

$$\alpha = \frac{2\left(\frac{h}{R_0}\right)}{1 - \left(\frac{h}{R_0}\right)}$$

where $0 \le \frac{h}{R_0} \le \frac{1}{3}$ or $0 \le \alpha \le 1$;

$$C_a = \frac{1}{\sqrt{3}} + \left(1 - \frac{1}{\sqrt{3}}\right) e^{-\ln\left[10^3\left(\sqrt{3}-1\right)\right]\alpha} \quad \text{where } 1/\sqrt{3} \le C_a \le 1;$$

and

$$\frac{p_r}{\sigma_u} = \frac{\left(\ln \frac{2}{\left(2 - \frac{h}{R_0}\right)}\right)^n}{n^n} \quad \text{where } \frac{p_r}{\sigma_u} \le 1.$$

Thus, the complete form of the friction coefficient can be written as

$$\mu = \frac{2\left(\frac{h}{R_0}\right)}{1 - \left(\frac{h}{R_0}\right)} \cdot \left[\frac{1}{\sqrt{3}} + \left(1 - \frac{1}{\sqrt{3}}\right) e^{-\ln\left[10^3\left(\sqrt{3}-1\right)\right]\frac{2\left(\frac{h}{R_0}\right)}{1-\left(\frac{h}{R_0}\right)}}\right] \cdot \frac{n^n}{\left(\ln \frac{2}{\left(2 - \frac{h}{R_0}\right)}\right)^n} \tag{29}$$

which is a function of strain hardening exponent n and interference ratio h/R_0.

2.6 Constraints in the proposed friction model

From Eq. (22) or Eq. (23), $p_r \le \sigma_u = Kn^n$,

$$p_r \le \sigma_u \tag{30}$$

or

$$K\left(\ln \frac{2}{\left(2 - \frac{h}{R_0}\right)}\right)^n \le Kn^n \tag{31}$$

Table 1. The relationships among n, $(h/R_0)_{\max}$, α_c and p_r/K.

n	0.05	0.15	0.18232	0.35	0.55
$(\frac{h}{R_0})_{\max}$	0.09754	0.27858	1/3	1/3	1/3
α_c	0.21616	0.77232	1	1	1
$\frac{p_r}{K}$	$0.05^{0.05}$ $= n^n$	$0.15^{0.15}$ $= n^n$	$0.18232^{0.18232}$ $= n^n$	0.55118 $< n^n$	0.39216 $< n^n$

The limiting condition of the above inequality can be written as

$$\ln \frac{2}{\left(2 - \left(\frac{h}{R_0}\right)_{\max}\right)} = n \tag{32}$$

where $(h/R_0)_{\max}$ is the maximum interference ratio corresponding to the condition of $p_r = \sigma_u$ for a particular critical value n. The critical value of $(h/R_0)_{\max}$ should be less than 1/3, the geometrical constraint. Additionally, the limiting condition based on Eq. (32) can also be in terms of n,

$$\left(\frac{h}{R_0}\right)_{\max} = 2\left(1 - e^{-n}\right) \tag{33}$$

meaning that each n has a critical value of $(h/R_0)_{\max}$ for the condition of $p_r = \sigma_u$. Therefore, the critical contact area ratio, α_c, corresponding to $(h/R_0)_{\max}$ can be obtained as

$$\alpha_c = \frac{2\left(\frac{h}{R_0}\right)_{\max}}{1 - \left(\frac{h}{R_0}\right)_{\max}} = \frac{4\left(1 - e^{-n}\right)}{1 - 2\left(1 - e^{-n}\right)} \tag{34}$$

and should remain less than unity.

For the critical case of $(h/R_0)_{\max} = 1/3$ (*i.e.* $\alpha_c = 1$), a critical value of n can then be obtained from Eq. (32) that

$$n = \ln \frac{2}{\left(2 - \frac{1}{3}\right)} = \ln 1.2 = 0.18232 \tag{35}$$

This critical value of $n = 0.18232$ implies the following:

(1) if $n < 0.18232$, then $(p_r/\sigma_u) = 1$ at $(h/R_0)_{\max} < 1/3$ and $\alpha_c < 1$, *i.e.* the mean contact pressure p_r will first reach the maximum value (true tensile strength σ_u, the maximum deformation resistance of metal) before interference h reaching the maximum value of $h = R_0/3$; thus, the conditions of $(h/R_0)_{\max} = 1/3$ and $\alpha_c = 1$ do not exist in this case because the metal has been fractured before $h = R_0/3$;

(2) if $n = 0.18232$, then $(p_r/\sigma_u) = 1$ at $(h/R_0)_{\max} = 1/3$ and $\alpha_c = 1$ just holds; and

(3) if $n > 0.18232$, then $(p_r/\sigma_u) < 1$ at $(h/R_0)_{\max} = 1/3$ and $\alpha_c = 1$. Thus, p_r can continue increasing until $(p_r/\sigma_u) = 1$; however, $(h/R_0)_{\max} = 1/3$ and $\alpha_c = 1$ are still invariable. Within this period, friction stress remains constant because a hydrostatic stress state always occurred ($(h/R_0)_{\max} = 1/3$), but contact pressure p_r increased. Therefore, the friction coefficient will begin decreasing with contact pressure until $p_r/\sigma_u = 1$.

This discussion demonstrates the complex relationships

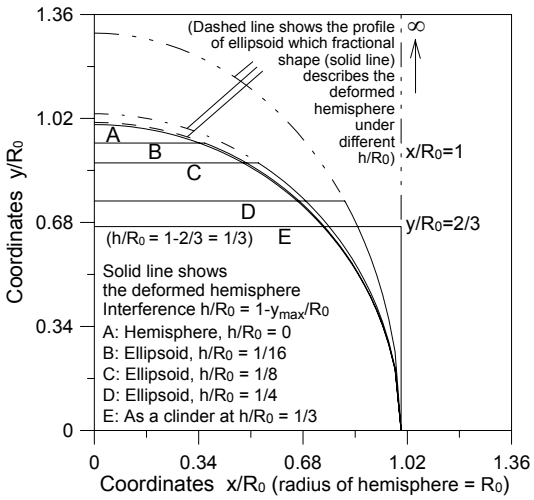

Fig. 7. The shapes before and after compression for the ellipsoid model.

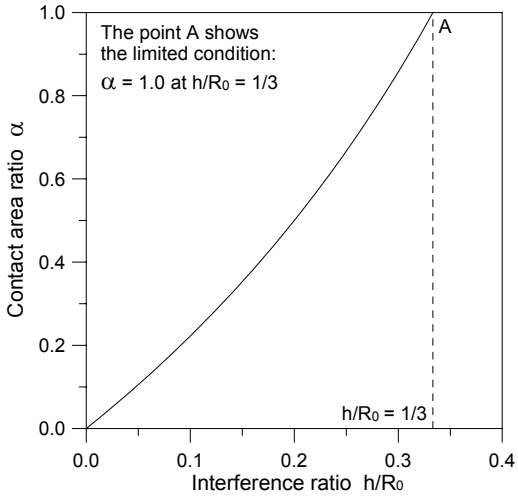

Fig. 8. Variation of contact area ratio α with interference ratio h/R_0.

among $(h/R_0)_{\max}$, (p_r/σ_u), α_c and n. These relationships are clarified using several cases of n in Table 1.

3. Results and discussions

The contact friction appears to be extremely difficult to determine. Therefore, a simple model for conceptually understanding friction is now proposed. The proposed model for evaluating friction coefficient μ is discussed as follows.

3.1 The profile of a deformable hemisphere against a rigid flat

The profile of a deformable hemisphere against a rigid flat is assumed a fractional shape of an ellipsoid, as described by Eq. (9). Fig. 7 shows the profile of the deformed hemisphere with h/R_0 from 0 (as a hemisphere) to 1/3 (as a cylinder). The predicted profile of deformed hemisphere is very similar

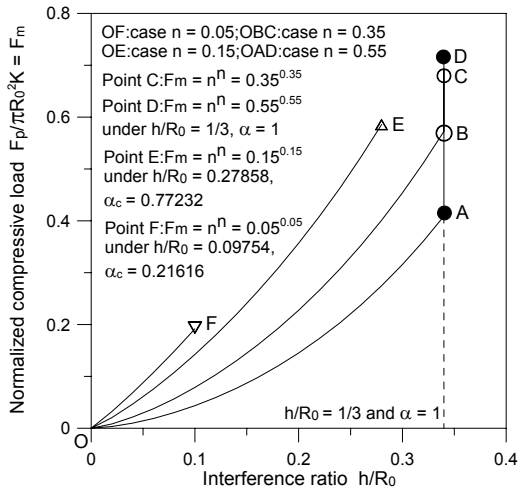

Fig. 9. Variation of normalized compressive load F_m with interference ratio h/R_0.

to the FE simulation results, such as the results by Jackson and Green [13] (Figs. 7 and 10), in which they are all the quadratic forms.

3.2 The contact area ratio $\alpha = A_r / A_a$

The contact area ratio, α, defined by Eq. (13) is utilized to measure the shearing effect under normal contact. Fig. 8 shows the contact area ratio, α, increases significantly as the interference ratio, h/R_0, increases, which shows a slightly increasing rate. In the final stage of compressive loading, α will approach unity when h/R_0 equals 1/3; it implies the contact friction condition reaches a beginning of sticking. The Fig. 4 of Etsion et al. [7] shows dimensionless contact area vs dimensionless normal load for three cases, which represents best fit of experimental data; and the trend of contact area ratio is very similar to the present result of Fig. 8 by the proposed model. Accordingly, the result of simulation obtained by Kogut and Etsion [14] (Fig. 8) shows dimensionless contact area vs dimensionless interference for different models, which trend with a slightly increasing rate is more similar to the present result of Fig.8; so does Jackson and Green [13] (Fig. 3) that shows dimensionless contact area vs dimensionless penetration depth for different models on a log scale.

3.3 The compressive load

The compressive load can be normalized and described by Eq. (25). It is a function of interference ratio h/R_0 and strain hardening exponent n. In terms of α and ε_e, Eq. (25) can be rewritten as

$$\frac{F_p}{\pi R_0^2 K} = \alpha \varepsilon_e^n \tag{36}$$

Based on the critical conditions of $\alpha \le \alpha_c \le 1$ and $\varepsilon_e \le n$,

$$\left(\frac{F_p}{\pi R_0^2 K}\right) \le n^n \tag{37}$$

Fig. 9 presents the theoretical effect of the interference ratio, h/R_0, on normalized compressive load F_m under various strain hardening exponents. The normalized compressive load increases significantly as the interference ratio, h/R_0, increases under various values for *n*. The trend of compressive load is very similar to the results of theoretical simulation conducted by Kogut and Etsion [14] (Fig. 9). In the proposed model, when $n < 0.18232$, the normalized load, F_m, will reach easily the maximum value, such that point F for $n = 0.05$ and point E for $n = 0.15$, and their $(h/R_0)_{\max}$ are always less than 1/3 such as $(h/R_0)_{\max} = 0.09754$ for $n = 0.05$ and $(h/R_0)_{\max} = 0.27858$ for $n = 0.15$ (Table 1). Conversely, when $n > 0.18232$, F_m will always be less than n^n as h/R_0 approaches 1/3 $(\alpha = 1)$, as in the case of $n = 0.35$ for point B ($F_m = 0.55118 < 0.35^{0.35}$) and $n = 0.55$ for point A ($F_m = 0.39216 < 0.55^{0.55}$). At this moment, $(h/R_0)_{\max} = 1/3$ remains invariable because a hydrostatic stress condition is induced; however, compressive loading can be subsequently increased to maximum contact stress, *i.e.* $\varepsilon_e = n$, which can be shown by point C ($F_m = 0.69251 = 0.35^{0.35}$) for $n = 0.35$ and point D ($F_m = 0.71978 = 0.55^{0.55}$) for $n = 0.55$. Clearly, all compressive loads reach the critical condition of n^n.

3.4 The adhesion factor C_a

An adhesion factor, C_a shown in Eq. (28), is proposed and utilized for evaluating the junction ability of asperities in sliding contact. Fig. 10 shows the distribution of the adhesion factor C_a with the contact area ratio α. The adhesion factor C_a decreases as the contact area ratio α increases. The adhesion factor C_a will decrease to a constant of $1/\sqrt{3}$ and then remain. Observing Figs. 5 and 10, $C_a = 1$ is clearly induced by an infinitely small contact (full junction or complete deformation energy concentration) at $\alpha \to 0$, which is a fracture case. Additionally, $C_a = 1/\sqrt{3}$ is induced by full contact (sticking or complete shearing) at $\alpha = \alpha_c = 1$, which is a shearing case.

3.5 Evaluation of friction coefficients μ

A simple and novel contact model for contact friction is proposed. The equation of friction coefficient is shown in Eq. (4) or Eq. (29). Fig. 11 shows the effects of the interference ratio, h/R_0, and strain hardening exponent, *n*, on the friction coefficient, μ. From the figure, there are four stages in trend for the distribution of friction coefficient, such as the line OCE (case $n = 0.55$), μ increases linearly with a large constant rate in the first stage, the rate of increase decreases in the second stage, increases with a low constant rate in the third stage, and then decreases with contact pressure under the invariable condition of $(h/R_0)_{\max}$ $(= 1/3)$ in the final stage. In the final stage, shown in line CE, the contact friction remains in a sticking state, indicating that friction stress retains a maximum shear stress τ_s and normal contact pressure can still increase to true tensile strength ($p_r/\sigma_u \to 1$). Notably, μ increases as *n* increases at a constant h/R_0. As $n <$ 0.18232, the friction coefficient will peak (point A for $n = 0.05$ and point B for $n = 0.15$) before full contact, *i.e.* $(h/R_0)_{\max} < 1/3$. Conversely, as $n > 0.18232$, the friction coefficient will always peak as h/R_0 approaches 1/3, as in the cases of point D for $n = 0.35$ and point C for $n = 0.55$. Thus, $(h/R_0)_{\max}$ will remain constant for a hydrostatic stress condition induced subsequently; however, compressive loading can be subsequently increased to maximum contact stress, $p_r = \sigma_u$, which is shown by point E as $n = 0.35$ and 0.55. At this moment, the friction coefficients will decrease to a constant $1/\sqrt{3}$ under the conditions of $\alpha = 1$, $C_a = 1/\sqrt{3}$ and $(p_r/\sigma_u) = 1$. For the case of $n = 0.18232$ shown in line OE, it is a special case in that the friction coefficient will directly increase to $1/\sqrt{3}$, which is a sticking state.

Finally, a comparison of friction coefficient between an experiment conducted by Hassan Mohamed et al. [15] and the calculated value of the proposed model is shown in Fig. 12. It is found that the calculated value is something larger than that determined experimentally. Therefore, the proposed contact model seems to overestimate the friction coefficient in this

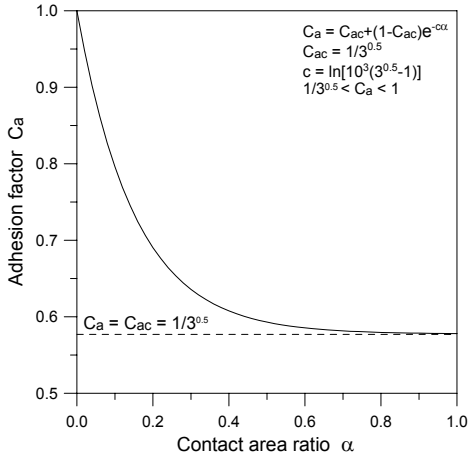

Fig. 10. Variation of adhesion factor C_a with contact area ratio α for contact adhesion.

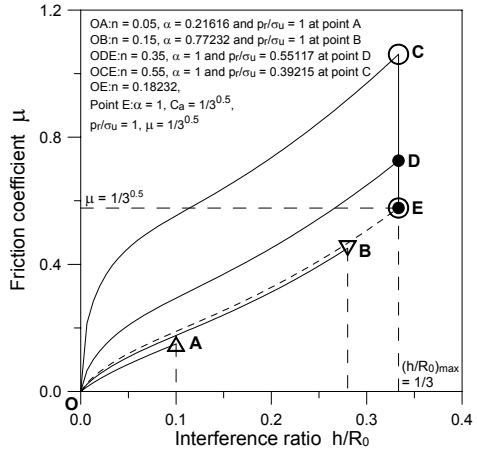

Fig. 11. Variation of friction coefficient μ with interference ratio h/R_0.

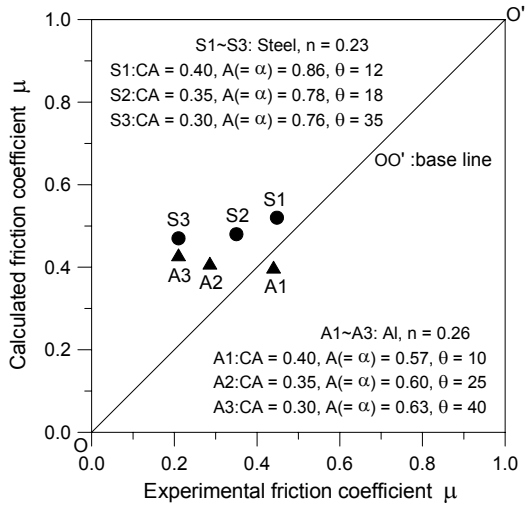

Fig. 12. Comparison between experimental and calculated friction coefficients, where the experiments was carried out by Hassan Mohamed *et al*. [15] in which "CA" is adhesion coefficient, "A" is contact area ratio and "θ" is contact angle.

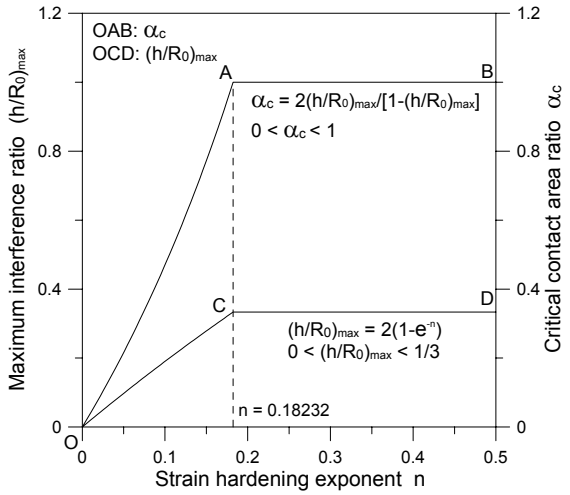

Fig. 13. Variation of maximum interference ratio $(h/R_0)_{\max}$ and critical contact area ratio α_c with strain hardening exponent n.

manner. However, the reason for the overestimation of the friction coefficient might be the increasing rates of the contact area ratio, shown in Fig. 8, for they obviously differ from the decreasing rates in other contact experiments, such as that by Wanheim and Bay [16] (Figs. 13 and 16) and Bay *et al*. [17] (Figs. 4 and 9).

3.6 The constraint of this contact modeling

From Eqs. (32) and (35), $n = 0.18232$ is found as a critical value. For $n < 0.18232$, the contact area ratio cannot reach full contact, *i.e.* $\alpha = 1$, because the contact pressure first reaches true tensile strength before full contact. This is in contrast to the case of $n > 0.18232$. Equation (33) shows the relationship between $(h/R_0)_{\max}$ and n and Eq. (34) shows the relationship between critical contact area ratio α_c and n. Both $(h/R_0)_{\max}$ and α_c increase as n increases until $n = 0.18232$ (Fig. 13). These values will always remain constant; thus, $(h/R_0)_{\max} = 1/3$ and $\alpha_c = 1$ as $n > 0.18232$.

Notably, the process factors interact in such a complex manner that they cannot be strictly considered in isolation. Although additional experience is needed, some practical conclusions are possible to further the understanding of the contact friction.

4. Conclusions

This work presents an evaluation of the friction coefficient for a model in which a rigid flat contacts a deformable hemisphere. Some practical conclusions are presented and a conceptual understanding of contact friction is provided. The following is a list of primary conclusions.

(1) The profile of a deformable hemisphere against a rigid flat is assumed to be the shape underneath an ellipsoid, significantly reducing the complexity in describing a deformed shape during compressive loading, which is a feature of this work. However, the interference ratio, h/R_0, should be less than 1/3. Clearly, the deformed hemisphere becomes a cylinder and a hydrostatic stress state is induced at the critical condition of $h/R_0 = 1/3$ (or $\alpha = 1$). The profile of deformed hemisphere agrees with FE simulation results, such as those obtained by Jackson and Green [13] (Figs. 7 and 10), in which all shapes have a quadratic form.

(2) The real contact areas of surface asperities play an important role in contact friction. The contact area ratio, α, significantly increases as the interference ratio, h/R_0, increases with a slightly increasing rate in this model. This trend agrees with experimental observations obtained by Etsion *et al*. [7] (Fig. 4) and the theoretical simulations such as those by Jackson and Green [13] (Fig. 3) and Kogut and Etsion [14] (Fig. 8).

(3) The compressive load is proposed as a function of the interference ratio, h/R_0, and strain hardening exponent n. As $n < 0.18232$, the normalized load F_m peaks before h/R_0 approaches 1/3. Conversely, as $n > 0.18232$, the normalized load is always less than n^n as h/R_0 approaches 1/3. Subsequently, $(h/R_0)_{\max} = 1/3$ will always keep invariable and then a hydrostatic stress state is induced; however, compressive loading can still increase to the critical condition such that contact stress reaches σ_u prior to surface fracture.

(4) A proposed adhesion factor C_a is used to measure the junction ability of asperities contact; the range of which is $1 \sim 1/\sqrt{3}$, which is another feature of this work. Clearly, $C_a = 1$ is induced by an infinitely small contact (full junction or complete deformation energy concentration) at $\alpha \to 0$, which is a fracture case in the proposed model. As $C_a = 1/\sqrt{3}$ is induced by full contact (a complete shearing state) at $\alpha = \alpha_c = 1$, which is a pure shearing case of sticking.

(5) A critical value of n is found such that the contact state

cannot reach full contact ($\alpha = 1$) as $n < 0.18232$, which is in contrast to the case of $n > 0.18232$. As $n > 0.18232$ and the contact state approaching full contact, the normal contact stress is still less than true tensile strength; thus, loading can increase until it equals true tensile strength. However, friction stress will always remain constant (the maximum shear stress for a hydrostatic stress state induced in this period) and result in a decreased friction coefficient. However, in the case of $n < 0.18232$, the friction coefficient simply increases as interference increases to a maximum value prior to surface facture. Additionally, the calculated friction coefficient is larger than that derived experimentally in previous studies. It may result from the increasing rates of the contact area ratio for which obviously differ from the decreasing rates in other contact experiments, such as that by Wanheim and Bay [16] (Figs. 13 and 16) and Bay et al. [17] (Figs. 4 and 9). However, the proposed model seems suitable for the modeling of micro contact friction because the proposed model is based on the micro contact of rough asperities. Under the micro scale, the friction coefficient increases with miniaturization that results from the size effect, has been verified by many researchers, such as Engel and Eckstein [18]. Although further study work is needed, some conceptual understandings of friction are possible.

The proposed friction concept may explain a number of observations and cover notions of friction used frequently.

Acknowledgment

The author would like to thank the National Science Council, Taiwan, R. O. C., for financially supporting this research under Contract No. NSC 97-2221-E-149-002. The author is grateful to Instructor C.-W. Yen for helpful discussions.

Nomenclature

A	:	Short axis of an ellipsoid
A_a	:	Apparent area
A_r	:	Real contact area
b	:	Long axis of an ellipsoid
c	:	A constant for C_a
C_a	:	Adhesion factor
C_{ac}	:	A constant ($=1/\sqrt{3}$)
F_p	:	Compressive load
F_m	:	Normalized compressive load
F_t	:	Friction force
h	:	Interference
h/R_0	:	Interference ratio
$(h/R_0)_{\max}$	:	Maximum interference ratio
K	:	Material constant
n	:	Strain hardening exponent
N	:	Normal force
p_r	:	Contact pressure
r	:	Radius before compression
R	:	Radius after compression
R'	:	Radius corresponding to an interference h
R_0	:	Radius of hemisphere
V_1	:	The squeezed volume at a certain interference h
V_2	:	The volume spread out around the contact plane ($= V_1$)

Greek symbols

α	:	Contact area ratio
α_c	:	Critical contact area ratio
$\varepsilon_r, \varepsilon_\theta, \varepsilon_z$	:	Strain at r, θ, z directions
ε_e	:	Effective strain
σ_e	:	Effective stress
σ_f	:	Fracture stress
σ_u	:	True tensile strength
τ_f	:	Friction stress
τ_s	:	Maximum shear stress
μ	:	Friction coefficient

References

[1] P. J. Blau, The significance and use of the friction coefficient, *Tribology International*, 34 (2001) 585-591.

[2] J. A. Greenwood and J. B. P. Williamson, Contact of nominally flat surfaces, *Proc. R. Soc. London*, Ser A, 295 (1966) 300-319.

[3] E. J. Abbott and F. A. Firestone, Specifying surface quality-a method based on accurate measurement and comparison, *Mech. Eng. Am. Soc. Mech. Eng.*, 55 (1933) 569-572.

[4] W. R. Chang, I. Etsion and D. B. Bogy, Static friction coefficient model metallic rough surfaces, *ASME*, *J. Tribol.*, 110 (1988) 57-63.

[5] L. Kogut and I. Etsion, A semi-analytical solution for the sliding inception of a spherical contact, *ASME*, *J. Tribol.*, 125 (2003) 499-506.

[6] L. Kogut and I. Etsion, A static friction model for elastic-plastic contacting rough surfaces, *ASME*, *J. Tribol.*, 126 (2004) 34-40.

[7] I. Etsion, O. Levinson, G. Halperin and M. Varenberg, Experimental investigation of the elastic-plastic contact and static friction coefficient of a sphere on flat, *ASME*, *J. Tribol.*, 127 (2005) 47-50.

[8] V. Brizmer, Y. Kligerman and I. Etsion, Elastic–plastic spherical contact under combined normal and tangential loading in full stick, *Tribology Letters*, 25 (2007) 61-70.

[9] A. Ovcharenko, G. Halperin and I. Etsion, Experimental study of adhesive static friction in a spherical elastic-plastic contact, *ASME*, *J. Tribol.*, 130 (2008) 021401.

[10] D. Cohen, Y. Kligerman and I. Etsion, The effect of surface roughness on static friction and junction growth of an elastic-plastic spherical contact, *ASME*, *J. Tribol.*, 131 (2009) 021404.

[11] F. P. Bowden and D. Tabor, *The Friction and Lubrication of Solids*, Clarendon Press, Oxford (1953).

[12] M. C. Shaw, *Metal Cutting Principles*, Oxford Press, Ox-

ford (1970).
[13] R. Jackson and I. Green, A finite element study of elastic-plastic hemispherical contact against a rigid flat, *ASME*, *J. Tribol.*, 127 (2005) 343-354.
[14] L. Kogut and I. Etsion, Elastic-plastic contact analysis of a sphere and a rigid flat, *ASME*, *J. Appl. Mech.*, 69 (5) (2002) 657-662.
[15] M. A.-N. Hassan Mohamed, N. G. El-Sebaie and K. Yamaguchi, An improved punch friction test in sheet metal forming, *Journal of the JSTP*, 42 (480) (2001) 31-37.
[16] T. Wanheim and N. Bay, A model for friction in metal forming processes, *Annuals of the CIRP*, 27 (1978) 189-194.
[17] N. Bay, T. Wanheim and B. Avitzur, Models for friction in metal forming, *Proc. NAMRC XVII* (SME) (1989) 372-379.
[18] U. Engel and R. Eckstein, Microforming-from basic research to its realization, *J. Mater. Process. Technol*., 125-126 (2002) 35-44.

Daw-Kwei Leu received M.S. and Ph. D. degrees in Mechanical Engineering from the National Taiwan University of Science and Technology in 1984 and 1995, respectively. Dr. Leu is currently a Professor at the Department of Mechanical Engineering, Technology and Science Institute of Northern Taiwan, Taipei, Taiwan. His main research field is on plasticity, metal forming process, microforming and contact friction.